

UC Berkeley

UC Berkeley Previously Published Works

Title

Automated segmentation of coronary vessels in angiographic image sequences utilizing temporal, spatial, and structural constraints

Permalink

<https://escholarship.org/uc/item/5bg91433>

Authors

O'Brien, James F
Ezquerro, Norberto F

Publication Date

1994-09-09

DOI

10.1117/12.185183

Peer reviewed

Automated Segmentation of Coronary Vessels in Angiographic Image Sequences Utilizing Temporal, Spatial and Structural Constraints

James F. O'Brien and Norberto F. Ezquerra

The Graphics, Visualization & Usability Center
College of Computing
The Georgia Institute of Technology

E-Mail: obrienj@cc.gatech.edu norberto@cc.gatech.edu

ABSTRACT

The methods presented here have been developed to perform the automated segmentation of coronary arterial structure from ciné sequences of biplanar x-ray angiograms. We introduce a methodology to impose an integrated set of constraints based on knowledge concerning the anatomical structure of the vascular system, temporal changes in position due to motion, and spatial coherence. Results are shown for data sets generated from both porcine and human studies.

1. INTRODUCTION

Radiographic imaging of coronary arterial structure plays a crucial role both in diagnosing and treating patients who are at risk of heart disease⁵. In order to exploit the information generated by current clinical methods in coronary arteriography, it is necessary for the physician to build a mental model of both the three dimensional (3D) arterial structure and of the non-rigid motion that this structure undergoes as it moves with the beating heart. This mental model must be constructed from sequences of two dimensional (2D) images obtained from the x-ray projection process (See *Figure 1*). The images shown in *Figure 2* represent a single pair of images from a typical sequence of sixteen pairs. The image data acquired is noisy and often very difficult to interpret, adding to the relative difficulty of the physician's decision-making task.

To facilitate this type of clinical decision-making process, much research has been done in the area of applying various computational algorithms for the purpose of generating a structural representation that is better suited for understanding and visualization by the physician. The primary focus of these algorithms has been to detect salient image features and then complete a segmentation of the angiographic 2D image. The segmented images can then be used to build and label a 3D model of the vascular system that can be interactively studied by the physician as it undergoes the motion associated with the beating heart's cycle^{9,1,4,10,11,8,2,14}.

Our approach attempts to make use of more information than that provided in a single image by considering the sequence of images as a set of discrete samples taken from an idealized continuous volume. (See *Figure 3.*) The result is a system that combines information contained in:

- ❑ Each individual image in a sequence,
- ❑ The temporal sequences as a spatiotemporal volume of information,
- ❑ *A priori* knowledge about the vascular structure, its dynamics, and
- ❑ *A priori* knowledge of the imaging technique and of the geometry of the environment.

2. DATA CHARACTERISTICS

The input to the segmentation system consists of two series of standard greyscale images (scale 0-255, 0 maps to black) taken from two different views. The two views are not taken simultaneously, but are interleaved with a separation time interval of $1/30$ th of a second. These two sequences can then be viewed as a discrete approximation of the continuous spatiotemporal motion of the arterial system as projected into two separate viewing planes. The details of the clinical protocols, imaging devices and preprocessing methods used to produce these

images are described in^{11,12}. The subsequent discussions are intended to underscore the salient characteristics of the acquired data in the context of the segmentation process.

In order to minimize ambiguity, it is useful to create a mathematical model of the input data in the following fashion. Each image is a matrix of dimensions $w \times h$, where w is the width of the image and h is the height. The pixel in the lower left corner of an image is designated as $I_{0,0}$ where I is some image.

There are two views, left (**L**) and right (**R**), which consist of the two distinct sequences of images through time, or *ciné sequences*, given by L_0, L_1, \dots, L_n and R_0, R_1, \dots, R_{n-1} .^{*} The first image in the sequence, **L**, is then referenced by L_0 and the

^{*}. Due to the interleave of the image acquisition process, there is one more left view than right view.

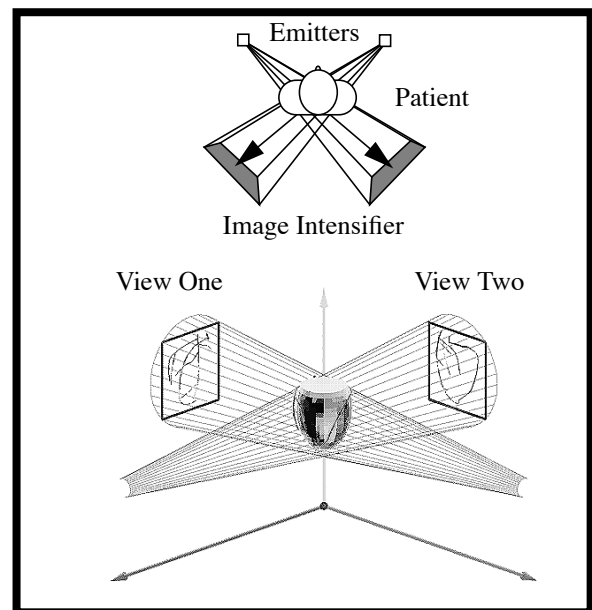


Figure 1. Biplanar Angiographic Projection. X-Ray emitters send out interleaved pulses of x-ray radiation. These rays are partially absorbed by dense tissues in the subject and by radio-opaque dye which has been previously injected into the patient's coronary arteries. The intensifiers can be positioned to yield different projected views of the arterial structure.

lower left pixel of the first image in the sequence \mathbf{L} is $L_{0,0,0}$, and in general $L_{t,x,y}$. Using this description, each ciné sequence is a volume referenced by the coordinate frame $(\hat{t}, \hat{x}, \hat{y})$ as shown in *Figure 3*.

3. METHODS

The process that performs the segmentation and extraction consists of a series of steps, each of which handles some specific subtask. *Figure 4* provides an illustration of this process, which is subsequently explained.

3.1 Initial preprocessing

The input images may have a high noise content which could cause errors during the segmentation process. To remove this type of noise, a low pass filter can be applied to the images as a preprocessing step. Because it is possible that this type of filtering may itself introduce errors, the original images are kept available and are used again during the final steps in the segmentation process.

Previous research^{7,11,12} has suggested several types of possible prefiltering. Among these are histogram equalization, thresholding and various edge enhancements. While we include prefiltering as a valid operation in *Figure 4*, the results reported here were obtained without prefiltering so that the results of the algorithms presented may be emphasized.

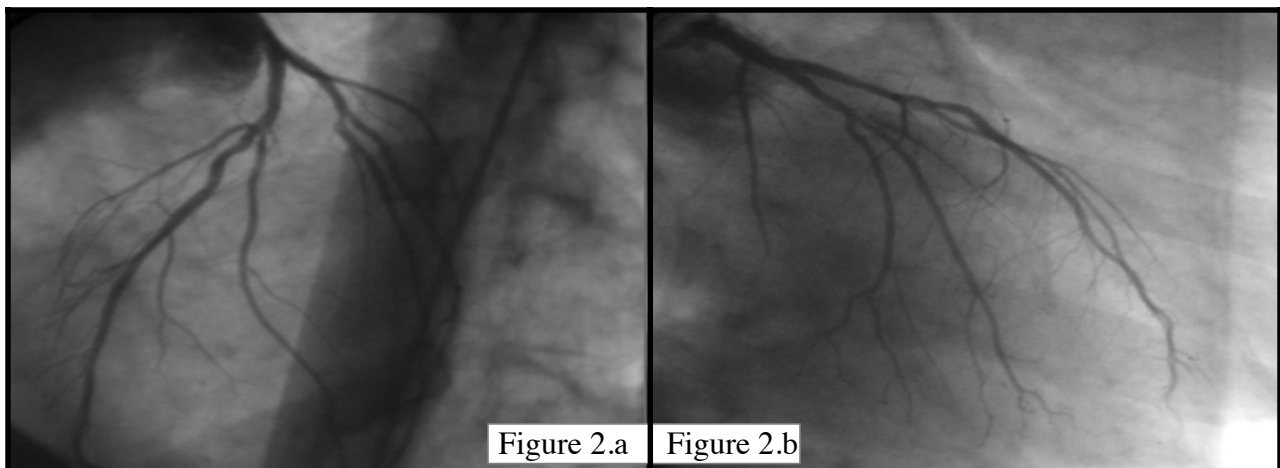


Figure 2. An angiogram pair showing a projection of the left coronary artery obtained from a study on a human subject. Figure 2.a shows the LAO view while figure 2.b show the RAO view.

3.2 Region growth and initial segmentation

Although the human eye can quickly locate the larger parts of the vessels in the input image, this task is not trivially implemented within the context of a computational model. There are several areas of the image background that, when locally viewed, are not readily distinguishable from vessel segments. For instance, physical objects present in the patient's chest, such as bone and muscle tissue, may appear in the x-ray projection as artifacts which resemble a blood vessel when viewed at a local scale. Our approach is to allow the user to select a point (or set of points) in the initial image of the ciné sequence which lies on the vascular structure, and to begin a search from this point. Currently this method of selecting a "seed point" is preferable because it induces the smallest amount of error into the final segmentation. While it does require user interaction, the time required is minimal. (Under one second per *ciné sequence* when a pointing device, such as a mouse, is utilized.)

Once an initial point, $s_0 = (0, x, y)$ which lies somewhere on the vessel structure is available, a search can be performed to expand a region outwards from this point. To do so, the following constraints are used:

- C1) The area which is part of the vessels is required to be "slightly darker" than the background.
- C2) For some sample area in the image, such as a square window, if the area is large enough, the ratio of vessel area to background area, a_v/a_b , will be less than some constant for each image.
- C3) The vessel segments are "elongated" structures.
- C4) The width of a healthy (non-stenotic) blood vessel changes "slowly".
- C5) The pixel values change "slowly" along the length of the connected vessels except where some object may intersect or occlude the blood vessel. (e.g. overlapping bifurcations.)

To expand a region once a seed point has been determined, first the set of points, Π , which are part of the region is initialized to the empty set, so $\Pi \leftarrow \emptyset$. Then, starting with the initial point, s_0 , each of its neighbor pixels within the image is examined. A test described below is applied to these neighbors and each neighbor pixel that passes the test is added to the set Π . The process is recursively continued until all members of Π have been expanded. To prevent infinite recursion, no pixel p with $p \in \Pi$ is examined more than once.

The test used in this process as mentioned above is arrived at in the following way. Let p be some point in a $d \times d$ sample area, assuming that p is part of some vessel segment of width w which runs through the sample area. Then, from C2, C3 and C4, the vessel area within the sample area can be approximated by the area of a parallelogram with width w , and height. If the vessel does not go thorough the sample area in a horizontal or vertical way we can still approximate the area by

$$a_v \leq w \times d \times \sqrt{2} \quad (\text{See Figure 6.})$$

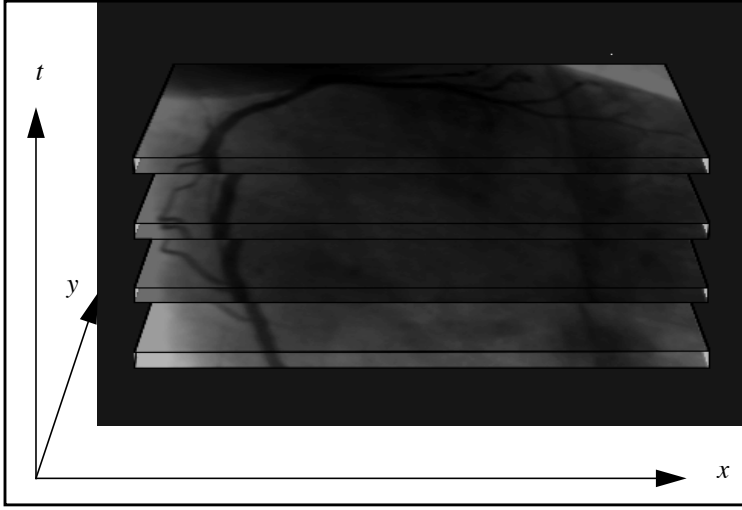


Figure 3. The image sequence forms a discretely sampled volume in the Cartesian coordinate frame (t,x,y) .

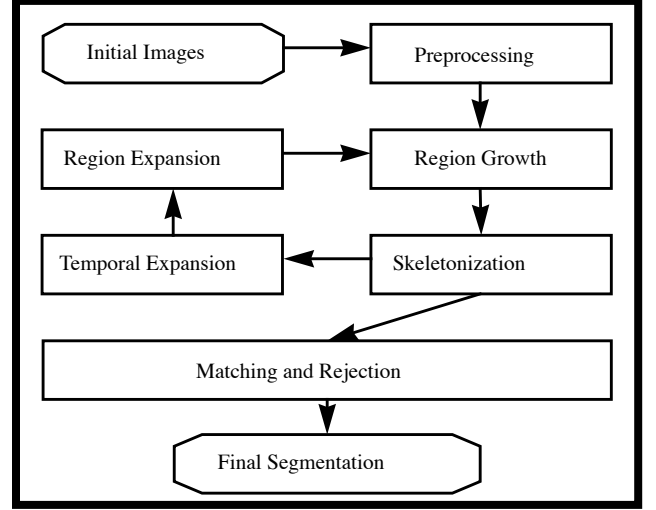


Figure 4. Schematic of data flow and processing within the segmentation system.

If p is part of a blood vessel, then the sum of the intensities across the sample area, i_s , should be approximately equal to the sum of the intensities across the area of the background, i_b , and the sum of the intensities of the pixels across the area of the blood vessel i_v , giving $i_s = \sum i_v + \sum i_b$. Since the values of i_v and i_b can not be computed directly, the approximations $\iota_v \approx i_v$, $\iota_b \approx i_b$ can be used in their place as follows:

$$i_v \approx \iota_v = i_p \times w \times d \quad (1)$$

$$i_b \approx \iota_b = \sum_{j \in \text{SampleArea}} i_j \quad (2)$$

Equation (1) utilizes the width approximation of a_v , and equation (2) the constraint C2. The approximation to the average intensity across the sampled area, \bar{i}_s , is then

$$\bar{i}_s \approx \bar{\iota}_s = \frac{\iota_v + \iota_b}{a_v + a_s} \quad (3)$$

where a_s is the area of the sample area. Finally, if the point in question, p , was in fact part of the blood vessel, then from C1 the inequality

$$\varepsilon i_p \leq \bar{\iota}_s \quad (4)$$

should hold, and the point passes the test. If (4) does not hold then the point in question fails.

3.3 Skeletonization processing

Once a region has been found which represents an initial approximation to the vessel structure, a set of operations is performed on the region in order to extract the set of pixels that roughly correspond to the points that form a center line of the blood vessels represented by the region. At this point, it is not necessary to have a continuous representation of the center line, nor would it be desirable. Ambiguities still exist in the extracted regions, and attempts to resolve them at this level in the process

are not likely to produce correct results. Therefore the centerline algorithm used is one which will not extract centers for ambiguous parts of the region. Because the resolution bifurcations and crossovers may not be possible from the information contained only in a single image, these features are treated as regions of ambiguity to be resolved during the construction of a center line graph in section 3.5.

The algorithm used to extract the centerline of the region begins with the set of pixels which make up the selected region, Π , and performs a balloon test on each member of the set. Those pixels which pass the subsequently described test become the set of pixels which makes up the centerline of the region, Ψ . The balloon test works as follows. Starting at the pixel to be tested, the algorithm expands a disk, of initial radius $r=1$ pixel, outward until some pixel is encountered which is not part of the region described by Π . When this occurs, it is called a *hit* as shown in *Figure 7*. If two hits occur on opposite sides of the disk at the same distance, then the point in question passes the test and is added to the set of center line points. Because this is a discrete pixel space, an error of one pixel is allowed. The shape of the disk used is an eight pointed star approximated by eight lines of length r extending from the center of the disk outward in each of the eight non-tertiary compass directions. In this algorithm, r is the parameter *radius* which varies as the disk expands. For those points which pass the test the final values of r is saved as an approximation of the vessel width at that point, $w = 2r \pm 1$.

3.4 Spatial region expansion

Although the vascular structure is a continuous network of vessels, the projection into the image plane may be broken up into disjoint segments by noise, image artifacts, structural defects (e.g., a stenosis) or other discontinuities. (See *Figure 8*) Additionally, it is possible that small vessels that should be detected will be partially obscured near larger vessels, hence the region test will not detect a small vessel which is too close to a much larger vessel. To adjust for this problem, the region must be spatially expanded and an extension to the region Π is built.



Figure 5. Extracted Regions superimposed on original image. Dark areas are initial extractions after filtering.

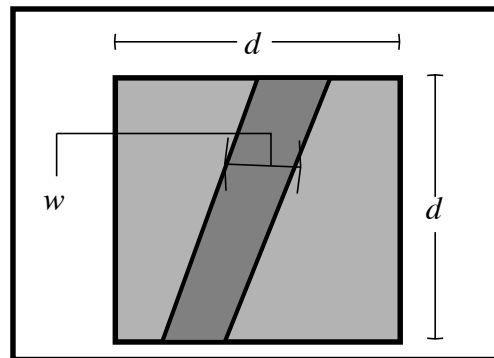


Figure 6. Note the area of any parallelogram constrained to lie in the region may have sides no longer than the diagonal of the region. This gives: $a_v < w \times d \times \sqrt{2}$

To perform this extension, the process starts with each center point, $c_i \in \Psi$ previously located by the balloon test, and searches the perimeter of a square area centered at that center point. The width of the square is equal to the sum of the width approximation at that center point, $w(c_i)$ and half the width of the search area, $d/2$, used from the region growth process. This is chosen so that the perimeter will be outside the influence of the already detected vessel segments. All the pixels on the perimeter are then tested using the region test as described above. For each one that passes, the region growth process is recursively started at that point. The new sub-regions generated in this way are then processed for center points and any new center points found are added to the set Ψ and used for further extension. This continues until no further spatial extension can be done, that is no perimeter points pass the region growth test.

In addition to the spatial expansion within the image plane, the expansion process is used to locate regions in the subsequent images of the sequence thus taking advantage of the temporal cohesion through the *ciné*-sequence. To do this, once the initial processing on the image I_0 has been done, the set of center points in I_0 is projected onto the image plane of I_1 . These center points are then used to perform a spatial expansion in I_1 . This process continues until no further expansion, as described previously, can be done in I_1 . This centers in I_1 are then projected into the next image so that in general I_i is used to perform the expansion into I_{i+1} . See (Figure 9).

3.5 Acceptance and Rejection of Regions

At this point in the process, each of the images contained in the input *ciné*-sequence has been separated into two parts, those selected regions which contain the vessels, and those areas which do not contain vessels. However, there is still no information

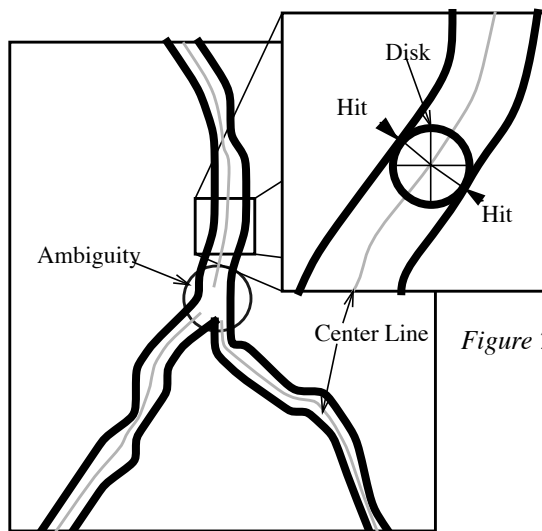


Figure 7. Center line detection and location of ambiguities within the extracted regions.

about how these sub-regions are related to each other: i.e. no explicit spatial or temporal connectivity exists in the detected data. Furthermore, some of the regions that have been selected may include errors, possibly corresponding not to blood vessels, but to noise or some part of the background. The goal of this part of the process is then:

- ❑ To establish an explicit spatial and temporal relationship among the sub regions,
- ❑ To identify and remove the erroneous regions, and
- ❑ To link the center points, Ψ , in such a way that a continuous directed skeleton of the arterial structure will be formed.

To do this, it is useful to view the data in the following manner. If each center point of the images in a sequence is viewed as a vertex node, $v \in V$, of a graph, $G = (V, E)$, and the sequence of images is viewed as discrete sampling of a volume, L or R , so that each vertex, $v \in V(G)$ exists in the domain of a function

$$f:V(G) \rightarrow (x, y, z), \tag{5}$$

$$x \in \{0..(w-1)\}, \quad y \in \{0..(h-1)\}, \quad z \in \{0..(n-1)\}$$

where w, h, n are the width of an image, height of an image, and number of images in a sequence respectively. The desired output of this stage in the process would then be a directed, acyclic connected graph for each image, $G_i=(V_i, E_i)$, where all vertices in G_i are reachable from some root vertex, $v_0 \in V_i$. Each vertex in the structure, $v \in V_i$, is mapped to a tuple (c, i, o) which corresponds to a center point, and inner edge and an outer edge, respectively. A depth first search of V_i from its root, v_0 , will fol-

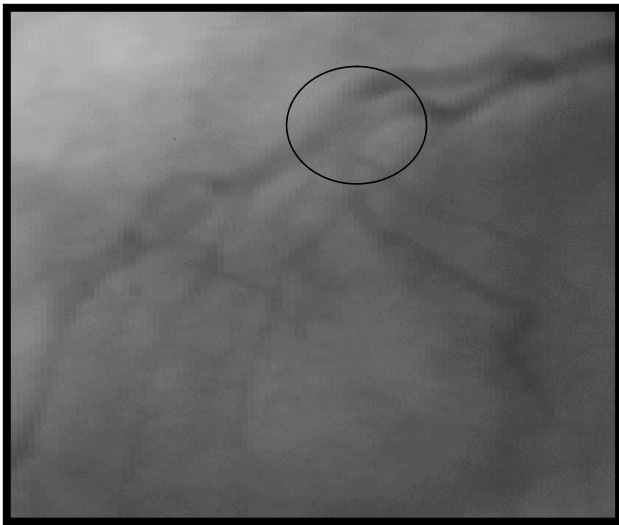


Figure 8. Although the actual arterial structure is continuous, areas may appear to be discontinuous in the image projection. This is particularly true where the arteries have become diseased.

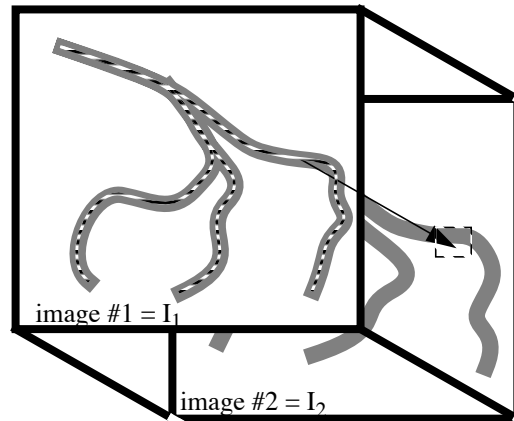


Figure 9. Center points of vessels found in an image of the sequence are projected into the image planes of subsequent images. The projected points will not necessarily hit a part of the vessel in the subsequent image as the structure moves with time. The projected point will, however, fall near to the new location of the vessel. The projected point is then used to begin the expansion process in the next image.

low the structure of the vascular network, with vertices who have more than one child mapping to a bifurcation, and nodes with no children mapping to vessel terminations. Furthermore a set of bidirectional edges, E_s , should be found which map each set of vertices, V_i , in image i to V_{i+1} in the next image. The final graph G is then:

$$G = (V, E) \quad (6)$$

$$V = \bigcup_{i=0}^{n-1} V_i \quad (7)$$

$$E = \bigcup_{i=0}^{n-1} E_i \cup E_s \quad (8)$$

There are, however, multiple graphs which could be fit to the description of G . To provide a means of selecting between them a, cost function, c , is defined for each edge in G , and the cost of a graph is given by the sum of costs of the edges in the graph. The cost function used here is the energy functional across the spline surface defined by the nodes in $G^{7,6}$. The desired output graph is then the one with the minimal cost value. The cost function is then defined as:

$$c(G) = \sum_{(u,v) \in E(G)} c(u,v) \quad (9)$$

$$c(u,v) = \alpha |x'(u,v)|^2 + \beta |x''(u,v)|^2 \quad (10)$$

So that the cost of adding an edge $e=(u,v)$ to a graph is a sum of the elasticity and flexibility across the surface at that edge^{7,11,6}.

Rejection of erroneous regions can be done at this stage by removing any edges which have cost functions significantly larger than the other edges in the graph. Any sub-set of vertices that is disjoint from the rest of the graph can then be removed. Additionally, the previously unresolved ambiguities can be mapped to the correct structural interpretation by the energy minimization process across the graph.

4. RESULTS AND CONCLUSIONS

The proposed system is a step towards fully automated segmentation of angiographic images, and the subsequent 3D reconstruction. These methods have been implemented within the context of an interactive image processing system. After each step in the process is applied by the computer, the user is able to interact with the system to accept or reject the results, or to make modifications to the extracted data. The image sequence shown in *Figure 10* and *Figure 11* shows the results of a session, which included about 30 minutes of user interaction, using a *ciné-sequence* generated from a human study. The images in column **A** are the original images obtained by X-ray angiography. The images in column **B** show the regions which are extracted after region growing and expansion have been done. The images in column **C** show the final segmentation after being passed through the rejection process and user filtering. The yellow points in *Figures 11b* and *11c* show the extracted center line pixels.

Finally, *Figure 11.d* shows the spatial projection of the structural graph superimposed on the original image. When running on a Silicon Graphics Indigo R4000, a 32 image sequence of 512x480 pixels data can be automatically processed in time between 3 to 5 minutes, depending on the input data.

To fully describe the vessel system, it is also necessary to have information about the edges as well as the centerline of the vessels. The edges formed by the region growing process become rough and jagged where the image quality is bad and are not acceptable for reconstruction. In their place, a more accurate set of edges should be found.

5. ACKNOWLEDGMENTS

The authors of this paper would like to thank the researchers at Emory Medical University for providing the raw data used in our work. This publication was supported in part by Grants 1 R01 HL 42052-01 from the National Institutes of Health and R 29 LM04692 from the National Library of Medicine.

6. WORLD WIDE WEB ACCESS

Higher resolution images and mpeg encoded versions of the image sequences shown in this paper are available as hypertext documents via mosaic. The URL is:

http://www.gatech.edu/gvu/medical_informatics/medinfo_home_page.html

If you are not familiar with mosaic or do not have access to this service, please contact obrienj@cc.gatech.edu for an alternative means for accessing these files.

6. REFERENCES

- 1 Coppini, G., Demi, M., Poli, M., and Valli, G., "An Artificial Vision System for X-Ray Images of Human Coronary Trees," *IEEE Transactions on Pattern Recognition and Machine Intelligence*, Vol. 15, No 2, pp 156-162, February 1993,
- 2 Elion, J., "A Knowledge-Based Expert System for the Automated Identification of Structures in Coronary Angiograms," *Computes in Cardiology Proceedings*, pp 201-204, 1988.
- 3 Fleagle, S., Johnson, M., Wilbricht, C., et. al., "Automated Analysis of Coronary Arterial Morphology in Ciné-angiograms: Geometric and Physiologic Validation in Humans," *IEEE Transaction on Medical Imaging*, Vol. 8, No. 4, December, pp. 387-400, 1989.
- 4 Garreau, M., Coatrieu, J. L., Collorec, R., Chardenon, C., "A knowledge-Based Approach for 3-D Reconstruction and Labeling of Vascular Networks from Biplane Angiographic Projections," *IEEE Transactions on Medical Imaging*, Vol. 10, No 2., pp 122-131, 1991.
- 5 Gould, K. L., "Assessing coronary stenosis severity: A recurrent clinical need," *JACC*, vol 8, pp. 91-94, 1986.
- 6 Kass, Michael, Witkin, A., Terzopoulos, D., "Snakes: Active Contour Models," *International Journal of Computer Vision*, Vol. 1, No. 3 pp. 211-221, 1987.

- 7 Hyche, M., Ezquerro, N., Mullick, R., "Spatiotemporal Detection of Arterial Structure using Active Contours," *Visualization in Biomedical Computing. SPIE* Vol. 1808. pp. 52-62, 1992.
- 8 Metz, C., "Determination of Three-Dimensional Structure in Biplane Radiography Without Prior Knowledge of the Relationship Between the Two Views," *Med. Phys.* 16(1), p45, 1989.
- 9 Miles, F., Nuttall, A., "Matched Filter Estimation of Serial Blood Vessel Diameters from Video Images," *IEEE Transaction on Medical Imaging*, Vol. 12, No. 2, June 1993. pp. 147-152, 1993.
- 10 Parker, D., "3D Reconstruction of the Coronary Arterial Tree from Multi-view Digital Angiography: A study of Reconstruction Accuracy," *Quantitative Coronary Arteriography*. p 226, 1991.
- 11 Peifer, John W., Ezquerro, N., Cooke, C., et. al., "Visualization of Multimodality Cardiac Imagery," *IEEE Transactions on Biomedical Engineering*, vol. 37, No. 8, pp 744-756, 1990.
- 12 Peifer, J., Mullick, R., Ezquerro, N., et. al., "Coronary Vasculature Visualization from Limited Angiographic Views," *Visualization in Biomedical Computing Proceedings*, 1990.
- 13 Rong, J. H., Coatrieux, J. L., and Collorec, R., "Motion Estimation in Digital Subtraction Angiography," *IEEE Engineering in Medicine & Biology Society 11th Annual International Conference Proceedings*, 1992.
- 14 Stansfield, Sharon, "ANGY: A Rule-Based Expert System for Automatic Segmentation of Coronary Vessels From Digital Subtracted Angiograms," *IEEE Transactions on Pattern Recognition and Machine Intelligence*. Vol. PAMI-8. No. 2. pp 188-198, March 1986.
- 15 Stevenson, D.J., Smith, L.D.R., and Robinson, G., "Working towards the automatic detection of blood vessels in X-ray angiograms," *Pattern Recognition Letters* 6, pp 107-112, 1987.

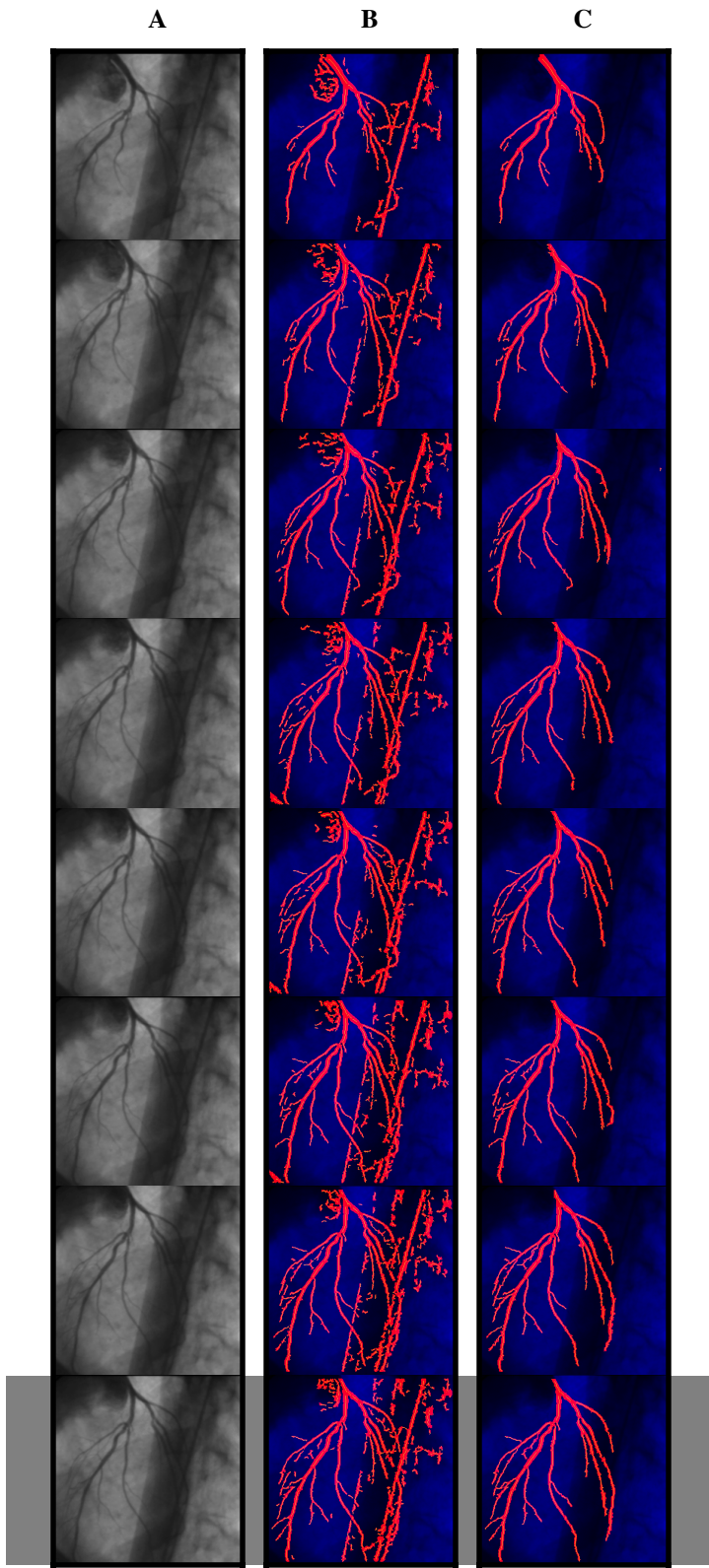


Figure 10.: This shows a sub-sequence of eight images from a human study. The images are 1/15 seconds apart progressing in time from top to bottom.

The images in column **A** are the original data obtained from the X-Ray angiography.

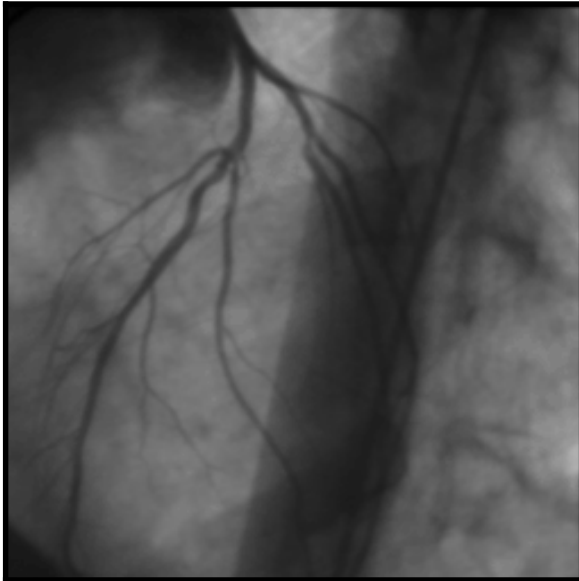
The images in **B** are the results after the system has performed an initial segmentation on the data set.

The images in **C** are the final results after being passed through the rejection process and user filtering.

The final set in the sequences, highlighted by the grey box, are shown in more detail in *Figure 11*.

Figure 11.: Detail of final frames from image sequences shown in Figure 10.

Figures 11.a, 11.b and 11.c are larger versions of the highlighted images shown in figure 10.a, 10.b and 10.c respectively.



11.A

Figure 11.a: Detailed view of original angiographic image.



11.B

Figure 11.b: Results after initial segmentation and expansion. Red areas are extracted regions. Green points are the corresponding center points.

Figure 11.c: The final results after being passed through the rejection process and user filtering.



11.C



11.D

Figure 11.d.: This image shows the final centerline graph superimposed on the original angiographic image.